Continuously controllable, wide-angle liquid crystal beam deflector based on the transversal field effect in a three-electrode cell

Boris Apter
Holon Institute of Technology
Department of Electrical and Electronic Engineering
Holon 58102, Israel
E-mail: apter@hait.ac.il

Eldad Bahat-Treidel
Ben-Gurion University
Department of Electro-Optical Engineering
Beer-Sheva 84105, Israel

Uzi Efron
Ben-Gurion University
Department of Electro-Optical Engineering
Beer-Sheva 84105, Israel
and
Holon Institute of Technology
Department of Electrical and Electronic Engineering
Holon 58102, Israel

Abstract. A controllable, refractive, electro-optical liquid crystal (LC) beam deflector is studied both theoretically and experimentally. The principle of operation of this device is based on a beam deflection from a large gradient of refractive index, generated in an LC layer by a transversal electric field, formed between two lateral electrodes, in a simple three-electrode LC cell. A continuous, controllable deflection of a Gaussian laser beam, focused into the narrow region at the electrode gap is demonstrated. Maximum deflection angles of ~18 to 25 deg, depending on the LC birefringence, as well as a high deflection efficiency of up to 98% are demonstrated experimentally, backed by a theoretical analysis.

[DOI: 10.1117/1.1911125]

Subject terms: liquid crystal; beam deflection; refractive index gradient; transversal field; fringing field.

Paper 040444 received Jul. 7, 2004; revised manuscript received Dec. 2, 2004; accepted for publication Dec. 3, 2004; published online May 11, 2005.

1 Introduction

Liquid crystal (LC) electro-optical devices are widely used in various areas of displays, optical communication, and information processing technology. Such LC devices, used as spatial light modulators, tunable filters, and controllable diffractive optical elements, offer several attractive features for beam-steering and beam-switching applications. The first LC-based beam-steering devices were described and evaluated in the mid-1970s. One type of such devices was a LC binary diffraction grating, patented by Borel et al.[1] This diffractive structure operated in an on-off mode and generated numerous diffractive orders. Another kind of beam-steering device was a refractive LC beam deflector, proposed by Fray and Jones.[2,3] This device deflected the linearly polarized, focused laser beam due to the electrically induced gradient of the LC's refractive index. This early LC-based beam deflector lacked the alignment layers routinely used in current LC devices, thereby severely limiting its continuous beam deflection capability (which was never demonstrated by this group). Although this device did provide a large deflection angle (about 20 deg), the very large thickness of the LC layer used required a very high operating voltage in the kilovolt regime. The thick layer used also resulted in very significant absorption (about 40%) and scattering losses.[2]

Further development of the LC beam-steering technology followed the path of blazed diffractive grating structure, based on the formation of the blazed phase profile in the LC layer, by the use of a multiple electrode structure onto which a periodically varying potential is applied.[4–6] The beam deflection angle is varied by changing the periodic voltage profile applied to the set of driving electrodes. The main drawback associated with these devices are the limitations imposed on both the diffraction efficiency and the maximum angular range (less than 2 deg in the visible), both being due to the fringing field effect that occurs in vicinity of the sharp spatial resets of the driving potential. The effect of the fringing and transversal* fields in LC devices was studied experimentally and theoretically in a number of early works.[7–14] In most of the cases studied, the lateral fringing fields at the electrode edges appear to degrade the performance of the LC spatial light modulators,[7–10,13,14] most notably, their resolution. However, in a few cases, such as in the in plane switching (IPS) devices,[11,12] the transversal fringing field is actually used to an advantage.

*We find it important to clarify the use of the two terms "fringing field" and "transversal field" used in this and other related works. Fringing field relates to the presence of a secondary, parasitic field at the edge(s) of the electrodes of a device, onto which a primary field is applied in a particular direction and level, consistent with the designed function of the device. Such would be the case of an LC spatial light modulator with the longitudinal fields between each of the pixel electrodes and the common counterelectrode defining the designed LC voltage drop in each of the pixels, while the by-product lateral fields at the edges of the pixel electrodes constitute the parasitic, unintended fringing fields. In a situation where the lateral or transversal field is applied in the region between the edges of the electrodes, such as in an in plane switching (IPS) device or in the beam deflector described in this paper, it is more appropriate to identify the field based on its directionality (e.g., "transversal") rather than as a "fringing" field. This is so since in this case, the field effect extends beyond the immediate vicinity of the electrode edges into the regions between the electrodes. This terminology is adopted throughout this manuscript, and we call such lateral, interelectrode fields transversal fields rather than fringing fields.

0091-3286/2005/$22.00 © 2005 SPIE

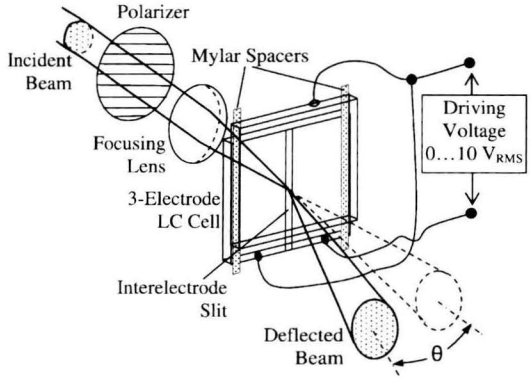

Fig. 1 Three-electrode LC beam deflector.

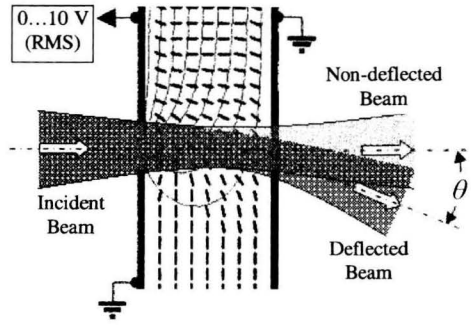

Fig. 2 Deflection of focused beam from the transversal-field-induced refractive inhomogeneity within the three-electrode LC cell.

Note also some other results on refractive LC beam deflectors here. An electrically induced LC prism,[15] which provides an extremely small deflection angles of about 25 arcsec, was demonstrated as a part of an adaptive optics system for imaging through the atmosphere. An electro-optic beam deflector was patented[16] based on an electrically controlled refractive index matching between the wedge-shaped grating structure and nematic LC. Finally, a multiple-deflection-stage beam deflector device[17] has also been described.

In this paper, we show that using modern LC technology, it is possible to significantly improve the operational features of the refractive beam deflector based on Fray' and Jones's idea.[2] A simple three-electrode LC devices with 12- and 24-μm-thick, optically uniform, low-absorption and nonscattering nematic LC layers were fabricated and evaluated. Due to the use of alignment layers, which induce an initially homogeneous alignment of the LC bulk,[18] combined with a drastically reduced LC thickness (by two orders of magnitude—as compared to Fray and Jones's work), the resulting refractive beam deflector demonstrates a continuous, controllable beam steering operation, a major reduction by factor of 100 of the operating voltage, as well as a significant reduction in the insertion losses. Thus, our proposed structure presents a competitive solution for beam steering compared to the blazed grating devices currently under study.

2 Device Description

The three-electrode LC beam deflector (Fig. 1) consists of a glass substrate with two transparent lateral electrodes, spaced 4 μm apart, and a third transparent grounded electrode, placed at the opposite glass substrate. The LC was homogeneously aligned using mechanically rubbed polyimide layers on both ITO-coated surfaces. A differential voltage corresponding to the required phase step change was applied to the lateral electrodes of this beam deflector. The gap between the glass substrates was filled with a nematic LC mixture. The large refractive index gradient generated by the transversal field between the two lateral electrodes resulted in the deflection of the incident, lens-focused, linearly polarized laser beam. Figure 2 shows a cross section of the three-electrode LC cell. The short bars within the LC layer represent the 2-D distribution of the LC director, i.e., the local direction of the optical axis of the nonuniform, birefringent LC, induced by the electric field. It is assumed that the incoming Gaussian laser beam is linearly polarized in the direction parallel to the initial alignment of LC (perpendicular to the interelectrode slit). As is shown in the following, for a Gaussian beam focused onto the LC layer, with its waist contained within the lateral gradient region of the extraordinary refractive index, a highly efficient, wide-angle deflection of the focused beam occurs, as shown qualitatively in Fig. 2.

3 Theoretical Consideration and Computer Simulation

To investigate the effect of the transversal field on the phase-step transition, we first studied a simplified model of the three-electrode LC cell configuration, consisting of two lateral electrodes with a differential voltage corresponding to the required phase step change and a third grounded electrode, placed at the opposite substrate. The computer simulations were performed for a nematic LC mixture MLC-6621-100 (Merck), which was subsequently used for the preparation of an experimental cell. The parameters of the LC layer used for the simulations were: $n_e = 1.7148$ and $n_o = 1.5082$ for the extraordinary and ordinary refractive indices, respectively; $\epsilon_{\parallel} = 6.7$ and $\epsilon_{\perp} = 3.6$ for the dielectric constants; director pretilt angle=2 deg; and cell thickness=12 μm. The simulation procedure was based on the numerical generation of 2-D distributions of LC director at various voltages applied between the two lateral electrodes. These 2-D distributions were used to calculate the variations of the LC refractive index. In this simulation phase we used the commercially available Autronic-Melchers **2DIMMOS** software.[19]

The bottom part of Fig. 3 shows the three-electrode configuration, with a 4-μm-wide gap between the lateral electrodes in a 12-μm-thick LC cell, along with the equipotential lines and the LC director distribution simulated at a driving voltage of 10 V. The top part of Fig. 3 shows the phase (retardation) profiles, $\Delta\varphi(x)$, calculated for normally incident, linearly polarized, 633-nm-wavelength monochromatic light. In this case, we neglected the ray-bending effects within the LC layer and the phase profiles were obtained by integrating the variations of the LC extraordinary refractive index along the straight rays' trajectories at various driving voltages, applied to one of the two lateral electrodes (the left electrode in Fig. 3). As we can see, both the swing of the phase profile $\Delta\varphi_{\max} - \Delta\varphi_{\min}$ and its slope in the vicinity of interelectrode slit $d\Delta\varphi/dx$ increase propor-

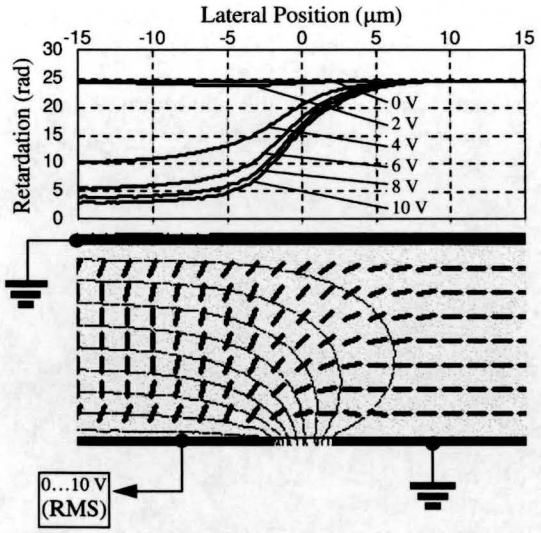

Fig. 3 Three-electrode LC cell configuration, director distribution, and equipotential lines at 10 V (bottom) and retardation profiles at various driving voltages (top).

tionately to the driving voltage. As we show shortly, the wide-angle deflection of the optical beam occurs because of this phase gradient. Let us assume that the Gaussian laser beam is focused onto the LC layer and that the focal waist of the beam is localized within the region of the strongest lateral gradient of the extraordinary refractive index, as shown in Fig. 2. The quasilinear, large-slope spatial phase profile formed is expected to result, similar to the linear phase modulation by a prism, in a wide-angle beam deflection. Depending on the relative size of the beam waist compared to the constant, linear index gradient region, a beam breakup may also occur. In the particular case where the beam waist is much narrower than the lateral extent of the refractive index inhomogeneity, an almost pure beam deflection will be observed.

We performed a simplified, 1-D analysis of this problem in the Fraunhofer diffraction approximation,[20] which yields, for the angular distribution of the far-field intensity,

$$I(\theta)\propto\left|\int_{-\infty}^{\infty}\exp\left(-\frac{x^2}{w_0^2}\right)\exp\left\{i\left[\Delta\varphi(x)-\frac{2\pi}{\lambda}x\sin\theta\right]\right\}\mathrm{d}x\right|^2, \tag{1}$$

where θ is the diffraction angle; w_0 is the effective half width of the beam waist within the LC layer; $\Delta\varphi(x)$ is the transversal-field-generated, voltage-dependent phase profile; and λ is the wavelength used. Using the Gaussian beam theory,[21] we can calculate approximately the waist width $2w_0$ within the LC layer, using the following relationships:

$$2w_0=\frac{4\lambda F}{\pi D}, \tag{2}$$

$$D=D_0\left[1+\left(\frac{L\alpha}{D_0}\right)^2\right]^{1/2}, \tag{3}$$

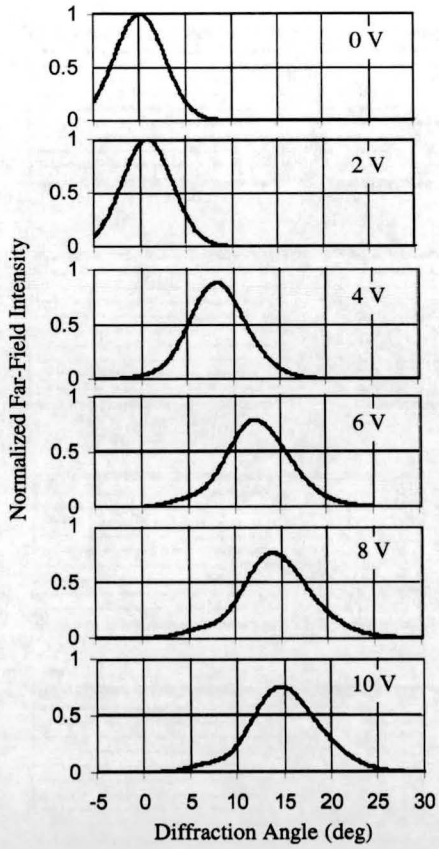

Fig. 4 Calculated far-field diffraction patterns at various driving voltages, for a 12-μm-thick, MLC-6621-100 mixture at $\lambda=633$ nm.

where F is the focal length or the lens used, D is the diameter of laser beam at rear focal plane of focusing lens, D_0 is the beam diameter at the output laser aperture, L is the distance between the laser aperture and rear focal plane of the focusing lens, and α is the initial beam divergence. Assuming a linear phase profile such that

$$\Delta\varphi(x)=\Delta\varphi_0+\beta(V)x, \tag{4}$$

where $\beta(V)$ is the voltage-dependent phase gradient, we can approximate the Fourier transform expression in Eq. (1) to yield the following estimate for the diffraction angle:

$$\theta\approx\lambda\beta(V)/2\pi. \tag{5}$$

Thus, the diffraction angle is approximately proportional to the phase gradient, the latter being proportional to the voltage applied. Figure 4 shows the far-field intensity distributions, calculated for the phase profiles, shown in Fig. 3, using Eqs. (1) to (3), with the following optical and geometrical parameters: $\lambda=633$ nm, $F=4$ mm, $D_0=0.63$ mm, $L=300$ mm, and $\alpha=1.3$ mrad. As we can see from Fig. 4, the maximum deflection angle is about 15 deg at a driving voltage of 10 V.

In the next step of the computer simulation, the 2-D LC director distributions were used for the numerical calculation of ray tracing in the LC layer. Our ray tracing procedure was based on the ray equation for a spatially inhomogeneous, anisotropic (birefringent) media.[22,23] Using this

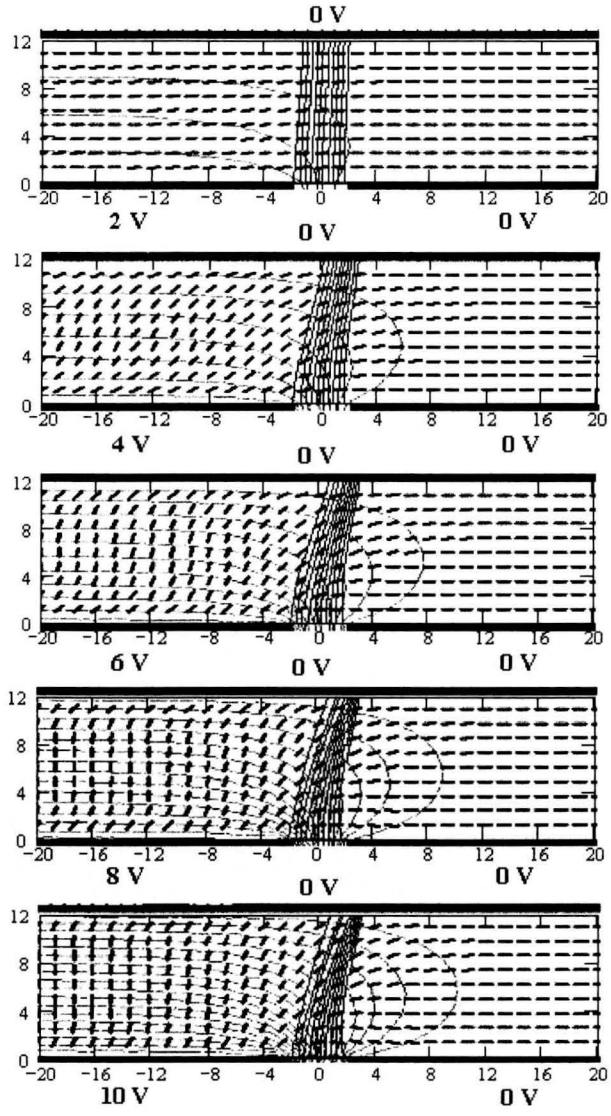

Fig. 5 Ray tracing within the LC layer at various voltages applied between two lateral (bottom) electrodes. (Horizontal and vertical scales are in micrometers.) The beam enters at the bottom and exits at the top plane.

method of ray tracing, we analyzed the effect of rays bending in the LC layer, caused by the transversal field. In these calculations, a focused Gaussian beam within the LC layer was approximated by a narrow pencil of initially parallel rays, normally incident on the LC layer. The pencil of rays was numerically traced through the LC layer. The results of the ray tracing are presented in Fig. 5, which shows the electrodes configurations, LC director distribution, the equipotential lines, and the rays trajectories. As we can see, the deflection angle of the ray pencil increases in proportion to the voltage difference applied to the lateral electrodes. The deflection angle attained was about 15 deg at an applied voltage of 10 V, which is in reasonable agreement with that obtained in the Fraunhofer diffraction calculation. Note that the ray-tracing results can be used to calculate the adjusted phase profiles by integrating the refractive index along the curved ray trajectories. These adjusted phase profiles can subsequently be used as the input data for further Fraunhofer diffraction calculations under the assumption that no ray crossing occurs within the LC cell and its output plane.

Now let us estimate quantitatively the maximum deflection angle $\theta_{\max}$ in the general case. Accordingly to Eq. (5):

$$\theta_{\max} \approx \lambda \beta_{\max} / 2\pi, \tag{6}$$

where

$$\beta_{\max} = (\mathrm{d}\Delta\varphi/\mathrm{d}x)_{\max} \tag{7}$$

is the maximum attainable slope of the phase profile. This slope can be estimated by

$$(\mathrm{d}\Delta\varphi/\mathrm{d}x)_{\max} \approx \left\{ (2\pi/\lambda) \int_0^d [\partial \Delta n(x,z)/\partial x] \mathrm{d}z \right\}_{\max}$$
$$\approx (2\pi/\lambda)(\Delta n_{\max}/\Delta X_{\mathrm{TF}})d, \tag{8}$$

where $\Delta n_{\max} = n_e - n_o$ is the LC birefringence, ΔX_{TF} is the effective extent of the transversal-field-induced refractive inhomogeneity, and d is the LC layer thickness. The effective extent ΔX_{TF} can be approximated from earlier fringing-field studies,[13,14] by

$$\Delta X_{\mathrm{TF}} \sim \Delta X_{\mathrm{FF}} \sim d, \tag{9}$$

where ΔX_{FF} is the lateral extent of the fringing field broadening of a phase profile. Substituting Eqs. (7) to (9) into Eq. (6), we finally get

$$\theta_{\max} \sim \Delta n_{\max}. \tag{10}$$

Thus, within this approximation, the maximum attainable deflection angle does not depend on the LC cell thickness but only on the optical birefringence of the LC material.

4 Experiment

The three-electrode LC cells were prepared with two glass substrates coated by indium-tin-oxide (ITO) conductive transparent layers. The ITO layer on one of the glass substrates was laser etched, yielding two transparent electrode sections isolated by a 4-μm-wide interelectrode gap. Both substrates were spin-coated by a polyimide layers and mechanically rubbed to produce an initial homogeneous alignment of the LC director, perpendicular to the inter-electrode isolating slit. A 12- or 24-μm-thick Mylar strips were used as spacers between the glass substrates. The cells were filled with Merck's nematic liquid crystal mixtures MLC-6621-100 or BDH-BL006. The cell was excited by a 1-kHz square-wave voltage driven by a function generator. The root mean square (rms) value of the driving voltage was varied from 0 to 10 V. The LC cell was mounted on a high-precision XYZ translation stage, for a precise positioning of the LC cell with respect to the focal waist of the laser beam. The linearly polarized laser beam (633-nm wavelength) focused onto the LC layer was then deflected by the transversal-field-generated inhomogeneity. A focusing lens with a focal length of 4 mm was used in the experimental setup, resulting in a focal waist size of $\sim$4 μm

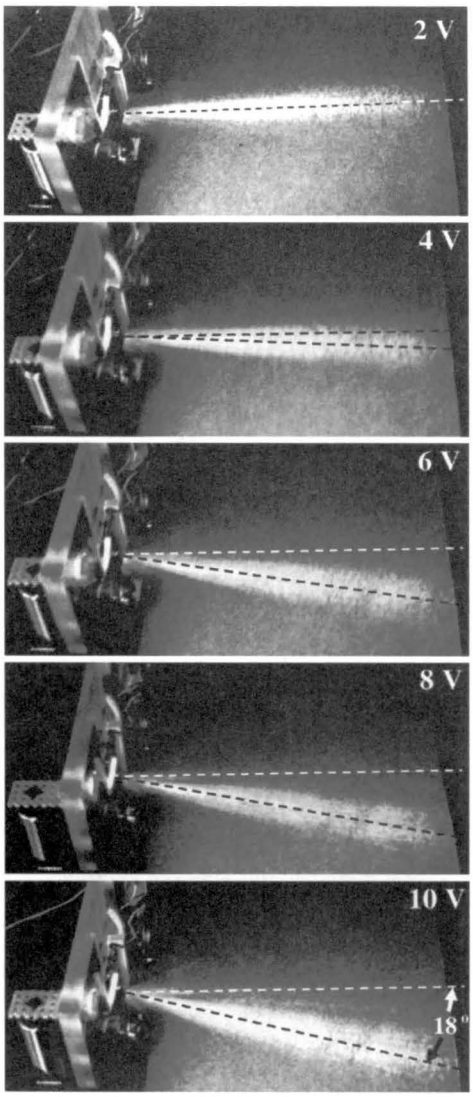

Fig. 6 Experimental demonstration of beam deflection operation at various voltages, for a 12-μm-thick, MLC-6621-100 mixture; $\lambda = 633$ nm; the maximum attainable deflection angle is about 18 deg at 10 V.

[calculated by Eqs. (2) and (3)]. This is significantly narrower than the $\Delta X_{TF} \sim d = 12$ or 24 μm lateral extent of the large-index gradient region.

The beam deflection effect was monitored in two ways. First, the deflected beam was visually traced using the rough, scattering surface of a paper sheet, as shown in Fig. 6. In addition to the beam deflection, a significant divergence of the deflected beam due its sharp focusing is clearly seen in Fig. 6. In the second method, the light spots of the deflected beam were observed on one side of an opaque screen, placed 5 cm from the LC cell, and were photographed from the other side by a digital camera. The photographs of the deflection patterns are shown in Fig. 7. As we can see from Fig. 7, the experimental diffraction patterns are in excellent agreement with the theoretically predicted patterns shown in Fig. 4. The results shown in Figs. 6 and 7 were obtained for an LC cell with a gap thickness of 12 μm, filled with MLC-6621-100 mixture.

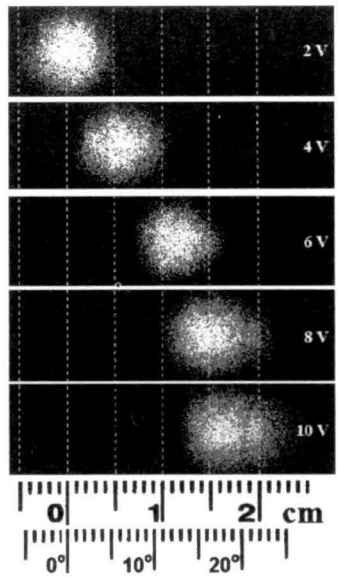

Fig. 7 Experimental deflection patterns versus driving voltages at distance of 5 cm from the 12-μm-thick, MLC-6621-100 mixture LC cell; $\lambda = 633$ nm.

We measured the intensity distribution of the deflected beam at various deflection angles. The intensity profiles were scanned by THORLABS INC's LC1 high-resolution CCD line camera, which consists of a 1-D 3000-element photodiode array with a 7-μm pitch. The sensor array was placed 11 mm from the LC cell. The intensity profiles were transferred from the camera to a personal computer via a parallel port. Figures 8 through 10 show the angular distribution of the output intensity at various driving voltages, applied between the two lateral electrodes of the three-electrode LC deflector. The experiments were performed with an MLC-6621-100 LC mixture, having cell gaps of 12 and 24 μm, and with a BDH-BL006 LC mixture with a cell gap of 12 μm. The physical properties of LCs used are shown in the insets of Figs. 8 through 10. As we can see

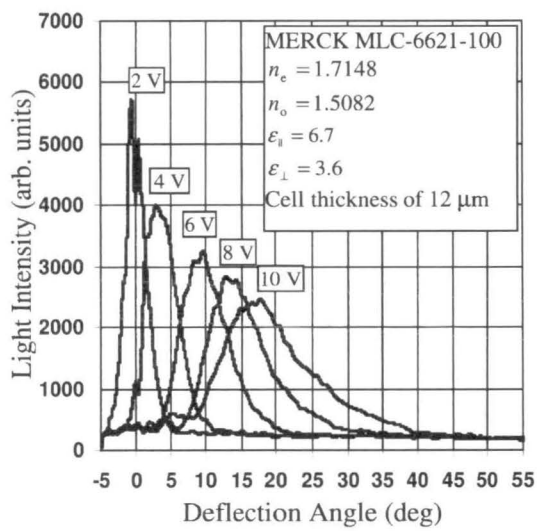

Fig. 8 Intensity profiles of deflected beam scanned by the CCD line camera at various voltages for the 12-μm-thick cell filled with the MLC-6621-100 LC mixture.

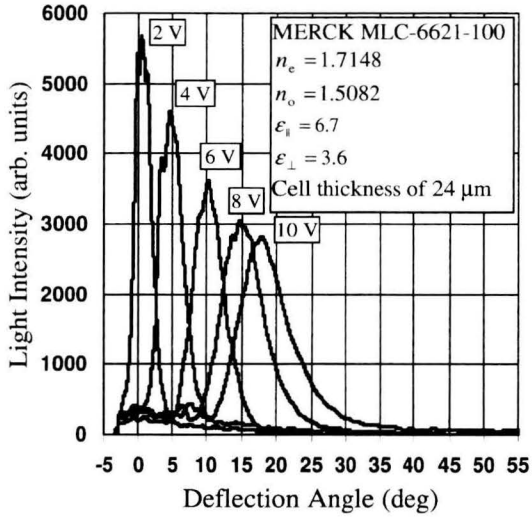

Fig. 9 Intensity profiles of deflected beam scanned by the CCD line camera at various voltages for the 24-μm-thick cell filled with the MLC-6621-100 LC mixture.

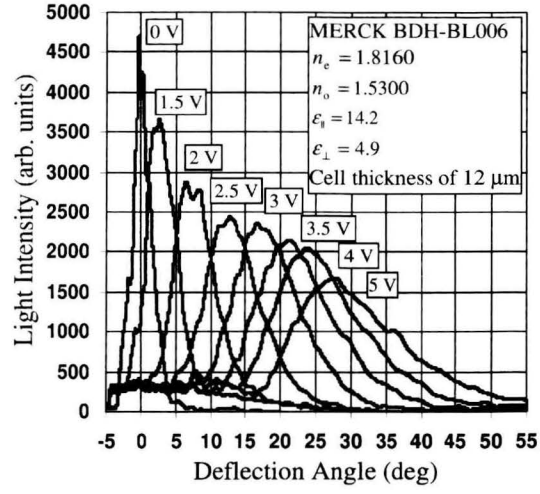

Fig. 10 Intensity profiles of deflected beam scanned by the CCD line camera at various voltages for the 12-μm-thick cell filled with the BDH-BL006 LC mixture.

from Figs. 8 and 9, the maximum intensity of the beam spot, deflected at the maximum angle (~18 deg at a 10-V driving voltage, for the MLC-6621-100 LC mixture) is approximately 50% of the maximum intensity of the unperturbed beam (transmitted through the nonactivated cell), with the spot width being proportional to the deflection angle. The beam deflection angle was found to be practically independent of the cell gap thickness, as predicted by the preceding qualitative analysis. For the deflector filled with BDH-BL006 LC material, the maximum deflection angle of about 25 deg was attained at a driving voltage of 5 V, as shown in Fig. 10. We note that the maximum angular deflection ratio of 25 deg/18 deg=1.388 for the two LC mixtures is approximately equal to their birefringence ratio (0.286/0.207=1.382), again in agreement with the prediction of our approximate analysis [Eq. (10)].

To estimate quantitatively the deflection efficiency of the device, the profiles of the intensity distributions of the 12-μm-thick cell, filled with the MLC-6621-100 LC mixture, shown in Fig. 8 were numerically integrated over the photodiode elements along the spatial extent of the beam spot for the different deflection states. The results of the integration show that the total energy of the deflected beam varies by only about 1 to 2% for the entire angular deflection range, within the accuracy of the photometric measurements performed. The absolute deflection efficiency is therefore approximately 98 to 99%. Note however, that the practical deflection efficiency is in fact lower due to the significant beam profile broadening at large deflection angles.

For the 12-μm-thick cells, filled with the MLC-6621-100 LC mixture, the total losses measured were below 8 and 14% in the nondeflected and the maximum deflection states, respectively. These values are in a reasonable agreement with the estimated losses due to multiple Fresnel reflections in the LC cell, since we have not used antireflective coatings. The increase of losses in the maximum deflection states may be due to the increase in the Fresnel reflection from the output glass substrate of the LC cell at larger incident angles. Note that we did not observe any light scattering phenomena in all three tested cells during the deflection operation.

The response time of the beam deflector was estimated by measuring the duration of the beam deflection process from a level of 10% deflection to 90% of the maximum deflection angle, by applying a transversal voltage step excitation of 10 V_{rms} to the LC cell. The deflection times of the 12- and 24-μm-thick cells were 140 ms and 540 ms, respectively. This experimental data is in a good agreement with the well known quadratic thickness dependence of the response time, in parallel aligned nematic LC cells.

Finally, for completeness, we also analyzed both experimentally and theoretically the case where the beam waist extends beyond the inhomogeneous index gradient region. This was done using the same experimental setup, but with an 8-mm-focal-length focusing lens, replacing the 4-mm one previously described. In this case, the theoretically expected beam breakup was indeed observed, again with an excellent agreement between the theoretical and experimental output intensity profiles.

5 Conclusion

A large phase gradient generated by the application of a transversal field between two lateral electrodes in a three-electrode LC cell was used to continuously deflect in a controlled manner, an incident optical beam with maximum deflection angles as large as 25 deg at high deflection efficiency. The advantages of this deflection method compared to that of the diffractive LC-blazed grating are the much simpler device structure and voltage driving scheme, as well as the much larger deflection angle attainable. The main disadvantage is the necessity to focus the beam into the narrow region of the phase gradient at the electrode gap, which in addition to the added difficulty in beam focusing, also results in a significant increase in the divergence of the deflected beam.

Acknowledgment

The partial support of this work by the Israel Science Foundation (ISF) is gratefully acknowledged.

References

1. J. Borel, J. C. Deutsch, G. Labrunie, and J. Robert, "Liquid crystal diffraction grating," U.S. Patent No. 3,843,231 (Oct. 22, 1974).
2. A. F. Fray and D. Jones, "Large-angle beam deflector using liquid crystals," *Electron. Lett.* **11**(16), 358–359 (1975).
3. A. F. Fray and D. Jones, "Liquid crystal light deflector," U.S. Patent No. 4,066,334 (Jan. 3, 1978).
4. R. M. Matic, "Blazed phase liquid crystal beam steering," in *Laser Beam Propagation and Control*, H. Weichel and L. F. DeSandre, Eds., *Proc. SPIE* **2120**, 194–205 (1994).
5. P. F. McManamon, T. A. Dorschner, D. L. Corkum, L. J. Friedman, D. S. Hobbs, M. Holz, S. Liberman, H. Q. Nguyen, D. P. Resler, R. C. Sharp, and E. A. Watson, "Optical phased array technology," *Proc. IEEE* **84**(2), 268–298 (1996).
6. D. P. Resler, D. S. Hobbs, R. C. Sharp, L. J. Friedman, and T. A. Dorschner, "High efficiency liquid crystal optical phased array beam steering," *Opt. Lett.* **21**(9), 689–691 (1996).
7. M. Bouvier and T. Scharf, "Analysis of nematic liquid crystal binary gratings with high spatial frequency," *Opt. Eng.* **39**, 2129–2137 (2000).
8. J. H. Kulick, J. M. Jarem, R. G. Lindquist, S. T. Kowel, M. W. Friends, and T. M. Leslie, "Electrostatic and diffraction analysis of a liquid crystal device utilizing fringing fields: applications to three-dimensional displays," *Appl. Opt.* **34**(11), 1901–1922 (1995).
9. G. Panasyuk, D. W. Allender, and J. Kelly, "Approximate description of the two-dimensional director field in a liquid crystal display," *J. Appl. Phys.* **89**(9), 4777–4786 (2001).
10. E. Hallstig, J. Stigwell, M. Lindgren, and L. Sjokvist, "Laser beam steering and tracking using a liquid crystal spatial light modulator," in *Laser Systems Technology*, W. E. Thompson and P. H. Merritt, Eds., *Proc. SPIE* **5087**, 13–23 (2003).
11. M. Oh-e and K. Kondo, "Electro-optical characteristics and switching behavior of the inplane switching mode," *Appl. Phys. Lett.* **67**(26), 3895–3897 (1995).
12. M. Oh-e, M. Yoneya, and K. Kondo, "Switching of negative and positive dielectro-anisotropic liquid crystals by in-plane electric fields," *J. Appl. Phys.* **82**(2), 528–535 (1997).
13. B. Apter, U. Efron, and E. Bahat-Treidel, "On the fringing field effect in liquid crystal beam steering devices," *Appl. Opt.* **43**(1), 11–19 (2004).
14. U. Efron, B. Apter, and E. Bahat-Treidel, "Fringing field effect in liquid crystal beam steering devices: an approximate analytical model," *J. Opt. Soc. Am. A* **21**(10), 1996–2008 (2004).
15. G. D. Love, J. V. Major, and A. Purvis, "Liquid-crystal prisms for tip-tilt adaptive optics," *Opt. Lett.* **19**(15), 1170–1172 (1994).
16. G. Moddel, J. R. Wootton, G. Waldman, and D. L. Holder, "Electro-optic wedge structure for beam steering and method of manufacture," U.S. Patent No. 5,615,029 (Mar. 25, 1997).
17. O. Pishnyak, L. Kreminska, and O. D. Lavrentovich, "Digital beam steering device based on decoupled birefringent prism deflector and polarization rotator," NASA Technical Report NASA/TM-2004-213197, available electronically at http://gltrs.grc.nasa.gov (2004).
18. L. M. Blinov, *Electro-Optical and Magneto-Optical Properties of Liquid Crystals*, Chap. 4, Wiley, New York (1983).
19. Autronic-Melchers **2DIMMOS** software, http://www.autronic-melchers.com/index.htm.
20. B. E. A. Saleh and M. C. Teich, *Fundamentals of Photonics*, Chap. 3, Wiley, New York (1991).
21. B. E. A. Saleh and M. C. Teich, *Fundamentals of Photonics*, Chap. 4, Wiley, New York (1991).
22. Y. A. Kravtsov and Y. I. Orlov, *Geometrical Optics of Inhomogeneous Media*, Springer-Verlag, Berlin (1990).
23. B.-J. Liang, J.-J. Wu, C.-S. Lin, and C.-H. Wang, "Ray tracing in an inhomogeneous liquid crystal cell," *Jpn. J. Appl. Phys., Part 2* **39**(2B), L163–L165 (2000).

Boris Apter received his BA and MSc degrees in electrical and electronics engineering from the Far-Eastern State Ransport University, Khabarovsk, Russia, in 1982 in the fields of automatic control and telecommunication systems and his PhD degree in physics (applied optics) from the State Research Institute for Opto-Physical Measurements, Moscow, Russia, in 1990 in the field of optical non-destructive testing (optical tomography). Since 2000 he has been a researcher with the Department of Electrical and Electronics Engineering, the Holon Academic Institute of Technology, Israel. His research interests include optical tomography, wireless optical communication, and electro-optical diffractive structures.

Eldad Bahat-Treidel received his BSc degree in chemical engineering in 1996 and he is currently an MSc student in the Electro-Optics Engineering Department, the Ben-Gurion University of the Negev, Beer Sheva, Israel. He is currently participating in research on liquid crystal and beam-steering devices. Formerly, he was a photolithography engineer at Intel Fab18 in Qiryat-Gat, Israel. He has participated in two publications on liquid crystals and beam-steering devices.

Uzi Efron is an associate professor in the Electro-Optics Engineering Department, the Ben-Gurion University of the Negev, Beer Sheva, Israel. He also heads the OPTO_ULSI Laboratory at the Holon Institute of Technology. He is currently conducting research on liquid crystal devices, CMOS-ultra large scale integration (ULSI) technology, and image processing for applications in smart goggle/head-mounted display devices, low-vision aids, face recognition techniques, and beam-steering devices. He was formerly a principal scientist at the Hughes Research Laboratories in Malibu, California, where he conducted research in photoactivated and CCD-addressed liquid crystal light valves as well as multiple-quantum-well spatial light modulators, and their applications in projection/head-mounted displays, optical data processing, and adaptive optics. He has more than 140 publications and presentations in solid state physics, solid state, and very large scale integration (VLSI) devices, spatial light modulators, optical data and image processing, adaptive optics, and displays. He is the author and coauthor of eight edited books and three book chapters on the technology of spatial light modulators. He holds 22 issued patents and is a fellow of the Optical Society of America.